J. Nanoanalysis., 5(2): 91-97 Spring 2018

ORIGINAL RESEARCH PAPER

Solid state synthesis, crystal structure, evaluation of direct and indirect band gap energies and optimization of reaction parameters for $As_2Ni_3O_8$ nanomaterials

Alireza Hakimyfard*[*,1], Shahin Khademinia[2], Masumeh Rahimkhani[1]

[1] *Department of Basic Science, Jundi-Shapur University of Technology, Dezful, Iran*
[2] *Department of Inorganic Chemistry, Faculty of Chemistry, Semnan University, Semnan, Iran*

Received: 2018-02-20 Accepted: 2018-04-20 Published: 2018-06-30

ABSTRACT

Nanostructured $As_2Ni_3O_8$ samples were synthesized via facile solid-state reactions at 850 and 950 °C for 8h using As_2O_3, $Ni(CH3COO)_2.2H_2O$ and $Ni(NO_3)_2.6H_2O$ raw materials. The synthesized nanomaterials were characterized by powder X-ray diffraction (PXRD) technique and fourier-transform infrared (FTIR) spectroscopy. The rietveld analyses showed that the obtained materials were crystallized well in monoclinic crystal structure with the space group $P12_1/c1$. The lattice parameters of the targets were about a = 5.76 Å, b = 9.54 Å and c = 10.18 Å with β = 92.95 °. It was found that nickel nitrate created a highly crystalline and pure $As_2Ni_3O_8$ structure. However, nickel acetate created the target with lower purity and crystal phase growth; it produced the samples with smaller crystallite sizes. Reaction temperature changing showed that the parameter affected on the crystal growth of the obtained materials. The morphologies of the synthesized materials were studied by field emission scanning electron microscopy (FESEM) technique. Ultraviolet-visible spectra showed that the synthesized $As_2Ni_3O_8$ nanomaterials had strong light absorption in the ultraviolet-visible light region. The direct optical band gaps were 2.6 and 2.5 eV for S_1 and S_3, respectively. The data showed that the band gaps were decreased by increasing the reaction temperature. This is due to the increasing the crystallite sizes of the obtained materials.

Keywords: *$As_2Ni_3O_8$, Nanomaterial, Rietveld, Solid State Method*

How to cite this article

Hakimyfard AR, Khademinia S, Rahimkhani M. Solid state synthesis, crystal structure, evaluation of direct and indirect band gap energies and optimization of reaction parameters for $As_2Ni_3O_8$ nanomaterials. J. Nanoanalysis., 2018; 5(2): 91-97.
DOI: 10.22034/jna.2018.541865

INTRODUCTION

Nickel ortho-arsenate ($As_2Ni_3O_8$) is composed of the two As^{5+} and Ni^{2+} cations. The compound has two crystal structure including orthorhombic and monoclinic structures. When the compound crystallizes in the orthorhombic crystal structure, the space group and lattice parameters of the target are Cmca and a = 5.943, b = 11.263, and c = 8.164 Å, respectively. The space group and lattice parameters of the compound crystallized in the monoclinic crystal system are $P12_1/c1$ and a = 5.764, b = 9.559, and c = 10.194 Å, respectively. $As_2Ni_3O_8$ contains NiO and As_2O_5 in its crystal system. NiO is interested in its electrical, magnetic and catalytic properties. Nickel (II) oxide is used in several applications such as catalyst production, electrochromic films, fuel cell electrodes, gas sensors, and etc. [1-5]. As_2O_3 is used in some fields including wood reservoir, and production of arsenic organic materials for various applications [6-7]. There is only one method for the synthesis of $As_2Ni_3O_8$. The hydrothermal method has been used for the synthesis of the single crystal of the target. $Ni_3(AsO_4)_2.8H_2O$ was used as raw material in this method [8].

In the present study, a facile solid- state route is applied for the first time to synthesize nanostructured

* Corresponding Author Email: *ahakimyfard@jsu.ac.ir*

$As_2Ni_3O_8$ powders using As_2O_3, $Ni(CH_3COO)_2.2H_2O$ and $Ni(NO_3)_2.6H_2O$ at 850 and 950 °C for 8 h. Besides, there is no report on the studying the optical properties of the obtained materials. So, the direct optical band gaps using UV-Vis spectra are calculated and related to the reaction temperature and crystallite sizes of the obtained targets. FTIR analysis is also studied.

EXPERIMENTAL

General remarks

All chemicals were of analytical grade, obtained from commercial sources, and used without further purification. Phase identifications were performed on a powder X-ray diffractometer D5000 (Siemens AG, Munich, Germany) using CuKα radiation. The morphology of the obtained materials was examined with a field emission scanning electron microscope (Hitachi FE-SEM model S-4160). The elemental analyses of the obtained materials were examined with a Philips XL30 scanning electron microscope (Philips, Amsterdam, Netherlands). The surface area and pore volume and average nanoparticles size were calculated using the Brunauer-Emmett-Teller (BET) equation. Pore size distributions, pore volume and pore surface area were calculated by the Barrett-Joyner-Halenda (BJH) method. BET surface areas were acquired on a Beckman Coulter SA3100 Surface Area Analyzer. Absorption spectra were recorded on an Analytik Jena Specord 40 (Analytik Jena AG Analytical Instrumentation, Jena, Germany). FTIR spectrum was recorded on a Tensor 27 spectrometer (Bruker Corporation, Germany).

Synthesis of $As_2Ni_3O_8$ nanomaterials

In a typical synthetic solid state experiment, 0.198 g (1 mmol) of As_2O_3 (MW = 197.8 $gmol^{-1}$) and 0.297 g (1 mmol) of $Ni(NO_3)_2.6H_2O$ (MW = 290.7 $gmol^{-1}$) (S_1) or 0.248 g (1 mmol) of $Ni(CH_3COO)_2.2H_2O$ (MW = 248.0 $gmol^{-1}$) (S_2) were mixed in a mortar and ground until a nearly homogeneous powder was obtained. The obtained powder was added to a 25 mL crucible and treated thermally in one step at 850 °C for 8 h. When the reaction was completed, the crucible was cooled normally in the furnace to the room temperature. The obtained powder was collected for further analyses.

For the synthesis of S_3 and S_4, the synthesis procedures explained for S_1 and S_2, respectively, were used. In this case, the reaction temperature is 950 °C.

RESULTS AND DISCUSSIONS

Characterization

The phase composition of S_1, S_2, S_3, and S_4 were examined by powder X-ray diffraction technique. Fig. 1(a-d) shows the PXRD patterns of the

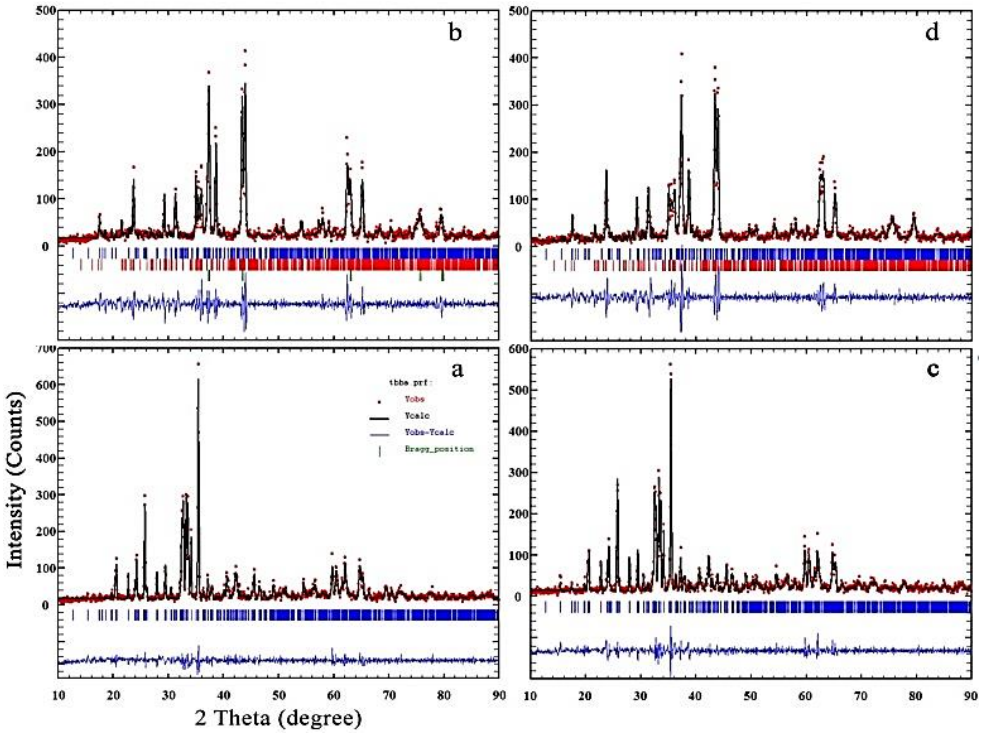

Fig. 1. PXRD patterns of a) S_1, b) S_2, c) S_4 and d) S_3.

obtained materials in the 2θ range 10-90° as well as the structural analyses performed by the *FullProf* program. The structural analyses were performed employing profile matching with constant scale factors. Red lines are the observed intensities; the black ones are the calculated data; the blue ones are the difference: Y_{obs}-Y_{calc}; and the Bragg reflections positions are indicated by blue and red bars for monoclinic phase of $As_2Ni_3O_8$ [9] and As_2O_3 [6, 7], respectively. The patterns have well fitted with monoclinic structure. The results showed that the patterns had a main $As_2Ni_3O_8$ crystal structure with space group $P12_1/c1$ [8].

Quantitative phase analysis was investigated with direct comparison method. In this method, we compared the experimental line intensity of the impurity phase (As_2O_3) from the mixture to a line from the main phase ($As_2Ni_3O_8$) in the mixture. For this purpose, we chose the peaks with the highest intensity for each phase at about 26.8˚ and 37.6˚ for As_2O_3 and $As_2Ni_3O_8$ (S_1-S_3) and 35.2˚ for $As_2Ni_3O_8$ (S_4), respectively. The phase comparison values are summarized in Table 1. Table 1 shows that the purity of the obtained $As_2Ni_3O_8$ is decreased at the two reaction temperatures 850 and 950 °C when nickel acetate is used as raw material. However, the data show that increasing the reaction temperature introduces a compound with higher purity only up to 3%. Besides, when nickel nitrate is used, the material with 100 % purity is obtained at the two reaction temperatures. Besides, the counts values are included in Table 1. The data show that the crystal counts values of the targets are related considerably to the raw material type. However, the data show that the obtained materials are crystallized better at lower reaction temperature. The rietveld parameters are also included in Table 1. The data show the goodness of the refinements. It is obvious that χ^2 value is smaller when the refinement is performed for S_1 and S_3. Besides, it is clear that the value for S_1 is smaller than that of S_3. It indicates that crystal growth amount is an important factor on the refinement goodness. Also, the other important factor is crystallite size. As will be mentioned in Table 2, the dislocation density and strain values are increased by decreasing the crystallite size. So, the rietveld refinement will be performed well when the crystallite size is increased.

Table 2 and (and graphically Fig. 2) shows the crystallite size data, dislocation density, strain, interplanar spacing (d) and cell parameters data for S_1 to S_4. The crystallite size data of the obtained nanomaterials is calculated by Scherrer equation (1):

$$D = \frac{K\lambda}{B_{\frac{1}{2}} cos\theta} \quad (1)$$

In this equation, D is the entire thickness of the crystalline sample, λ is the X-ray diffraction wavelength (0.154 nm), K is the Scherrer constant (0.9), $B_{1/2}$ of FWHM is the full width at half its maximum intensity and θ is the half diffraction angle at which the peak is located. The crystallite size data show that raw material type plays an important role to produce particles in nanometer size scale. The data included in Table 1 show that the crystallite sizes are decreased when nickel acetate is used as raw material. However, when the reaction temperature is increased, the value is increased when nickel nitrate is used as nickel source. Decreasing the D value for S_4 is maybe due to the faster decomposition of the organic part of nickel acetate. This can introduce a smaller particle size compared to that for S_2.

Table 1. Quantitative phase analysis for the obtained nanomaterials.

Sample	Rietveld parameters			Phase purity (%)	Counts
	R_{Bragg}	R_f	χ^2		
S_1	1.63	1.09	1.23	100	656
S_2	2.65	1.48	1.76	71	418
S_3	1.83	1.11	1.39	100	562
S_4	1.94	0.859	1.71	74	408

Table 2. Crystallographic data of the obtained materials.

Sample	2θ(°)	D(nm)	δ(lines/m^2)	ε	d_{Bragg}(Å)	d_{Calc}(Å)	a (Å)	b (Å)	c (Å)	Volume(Å^3)
S_1	37.65	43	5.41	0.81	2.3861	2.3870	5.76567	9.54803	10.184350	560.0
S_2	37.50	33	9.20	1.06	2.3958	2.3959	5.733498	9.583695	10.168968	558.0
S_3	35.26	83	1.45	0.79	2.5423	2.5466	5.764491	9.546424	10.186231	560.0
S_4	37.50	25	16.00	1.40	2.3958	2.3965	5.731564	9.585959	10.184628	559.0

The value of the dislocation density (δ (lines/m^2) $\times 10^{14}$) which is related to the number of defects in the crystal was calculated from the average values of the grain size (D) by the relationship given below:

$$\delta = \frac{1}{D^2} \quad (2)$$

The strain ($\varepsilon \times 10^{-3}$) values were determined with the use of the following formula:

$$\varepsilon = \frac{\beta_{hkl}\ cos\theta}{4} \quad (3)$$

The variation in the strain as a function of raw materials type and reaction temperature is included in Table 1. Increase in the strain with increasing the reaction temperature is probably due to the retrograde in the degree of crystallite of the obtained target. This is because of the deficiency of the crystals when the crystal sizes become smaller. So, the data in Table 1 indicate that the raw material type influences the crystallite size, strain and dislocation density values.

The interplanar spacing values are calculated using equations 4 and 5:

$$n\lambda = 2dsin\theta \quad (4)$$

$$\frac{1}{d^2} = \frac{1}{sin^2\beta}\left(\frac{h^2}{a^2} + \frac{k^2 sin^2\beta}{b^2} + \frac{l^2}{c^2} - \frac{2hl\cos\beta}{ac}\right) \quad (5)$$

The highest intensity peak at $2\theta \approx 37.50^{\circ}$, the (h k l) value of (0 4 0), and $\beta = 92.93^{\circ}$ are used in the above equation.

As we know, *sin* (92.93) is about 1, *cos* (92.93) is -0.051. So,

$$\frac{1}{d^2} = \left(\frac{16}{b^2}\right)$$

And

$$d = \left(\frac{b}{4}\right)$$

And for S_4, with using the peak at 2θ=35.26, the (h k l) value is (004). So

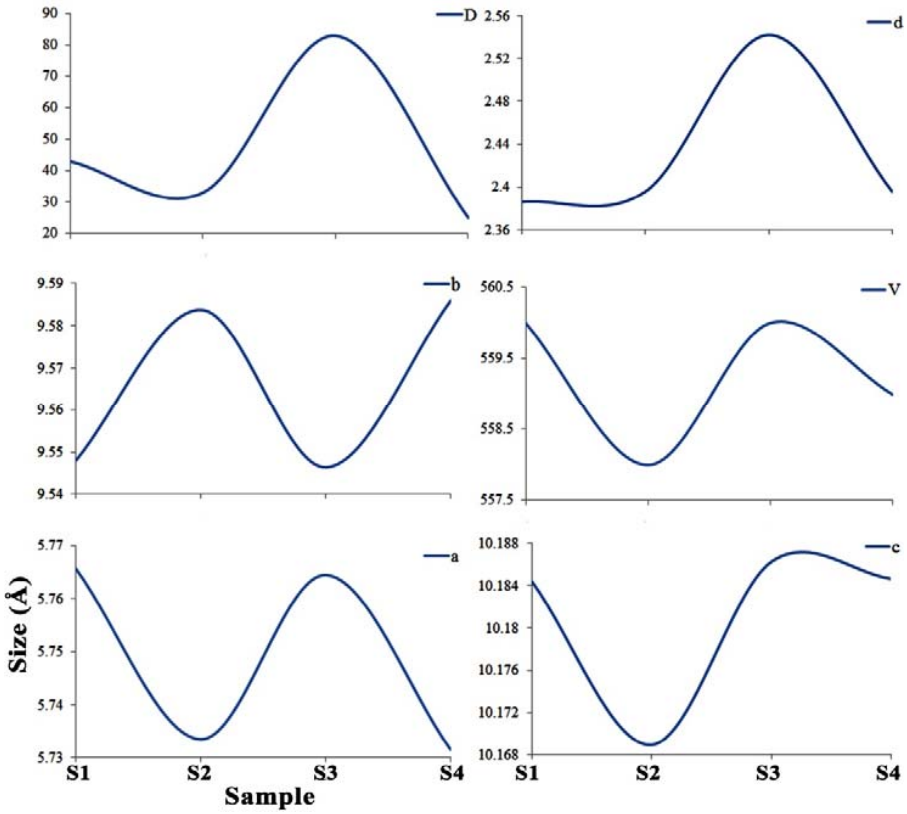

Fig. 2. Reined crystallographic data of the obtained samples.

$$d = \left(\frac{c}{4}\right)$$

Besides, the unit cell volume can be obtained from the bellow formula:

$$V = a.b.c.sin(\beta) \quad (6)$$

Where a and c are the lattice parameters and V is the cell volume.

The cell parameters values were calculated and refined by the rietveld analysis. The data show that the increasing/decreasing trend for parameters *a* and *c* is in reverse with parameter *b*. Because the trend for parameters a and c is in accordance with that for D values, so it is suggested that there is a preference in crystal growth to the *a.c* plane when the reaction time is increased to 950 ºC. Fig. 2 shows the summary data of the obtained crystallographic data schematically. The data show that the changing trends of the data are similar to each other's, except for parameter b.

Morphology analysis

Fig. 3 shows the FESEM images of the obtained nanomaterials. The images show that the morphology of the targets is sponge. It is clear that the sponge size of the two materials is homogeneous. However, the data show that the particle size of S_1 is smaller than that for S_3. The increasing the particle size is in accordance with the trend of the changing the crystallite size described in the PXRD analysis section. The images show that the particle sizes are about 50 - 70 nm for S_1 and 100 - 150 nm for S_3.

Textural analysis

The synthesized powders were characterized by their surface area, average pore size, and average pore volume. Prior to N_2-physical adsorption measurement, the samples were degassed at 150 °C for 120 min in the nitrogen atmosphere. So, the specific surface area (S_{BET}) of the obtained materials was determined with adsorption-desorption isotherms of N_2 at 77 K. The surface area, pore volume and average pore diameter of the synthesized materials are summarized in Table 3. From Table 3, it can be seen that the average surface area and pore volumes are about 4.669 $m^2\ g^{-1}$ and 0.0089 $cm^3\ g^{-1}$ for S_1, 3.251 and 0.0065 $cm^3\ g^{-1}$ for S_3, respectively. The data summarized in Table 4 shows that the specific surface area of pores of S_1 is larger than that of S_3 and the pore width of S_3 is larger than that of S_1. So, the investigated results of BET and BJH measurements suggest that the surface area of S_1 is larger than that of S_2. This observation is in good accordance with the FESEM images.

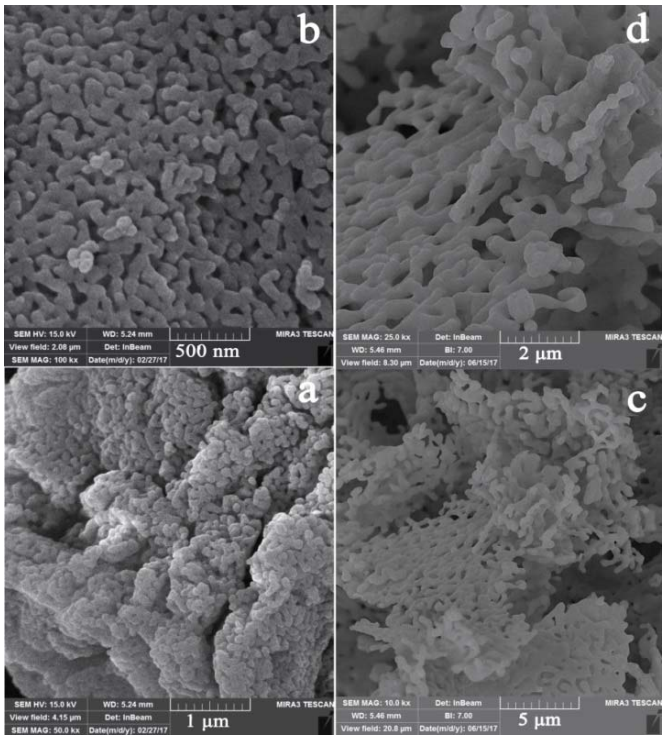

Fig. 3. FESEM images of a,b) S_1 and c,d) S_3.

Table 3. BET data for $As_2Ni_3O_8$ showing the textural properties of the obtained materials.

Sample	BET surface area (m^2g^{-1})	Pore diameter (Å)	Pore volume (cm^3g^{-1})
S_1	4.669	7.71	0.0089
S_3	3.251	8.93	0.0065

Table 4. BJH data for $As_2Ni_3O_8$ showing the textural properties of the obtained materials.

Property	S_1	S_3
BJH adsorption cumulative surface area of pores	6.184	5.34
BJH adsorption cumulative volume of pores	0.0104	0.0096
BJH adsorption average pore width (4V/A) (nm)	6.73	7.18

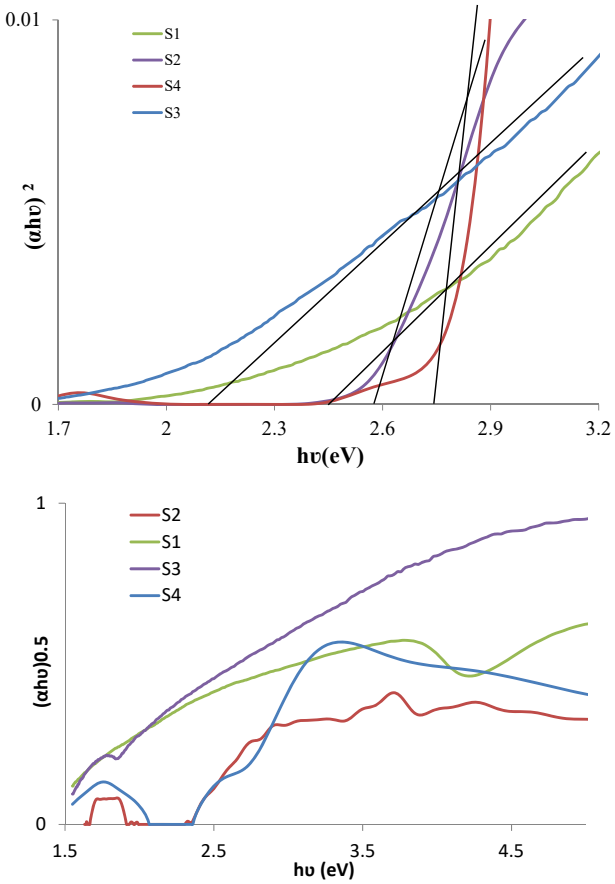

Fig. 4. Direct and indirect optical band gap energies plots of $(\alpha h\nu)^2$ and $(\alpha h\nu)^{0.5}$ versus hν (eV) of the obtained nanomaterials.

Optical Properties

The direct and indirect optical band gap energies of the $As_2Ni_3O_8$ nanomaterials obtained from UV-Vis absorption spectra are shown in Fig. 4. According to the results of Pascual *et al.* [9], the relation between the absorption coefficient and incident photon energy can be written as $(\alpha h\nu)^n = A(h\nu - E_g)$, where A is a constant and E_g is the direct band gap energy if n=2 and indirect band gap energy if n=0.5. The Band gap energies were evaluated from extrapolating the linear part of the curve to the energy axis. The direct optical band gaps were 2.50, 2.65, 2.30 and 2.80 eV for S_1, S_2, S_3, and S_4, respectively. The data show that the band gap energy values for the pure materials (S_1 and S_3) are smaller than those for the impure materials (S_2 and S_4). This can be due to the composite nature (As_2O_3 and $As_2Ni_3O_8$) of the obtained materials when nickel acetate is used as raw material. Besides, the value for S_3 is smaller than S_1. This can be due to the larger crystallite sizes of S_3 compared to S_1. This is due to the affect of D (nm) value in the calculation of the band gap energies.

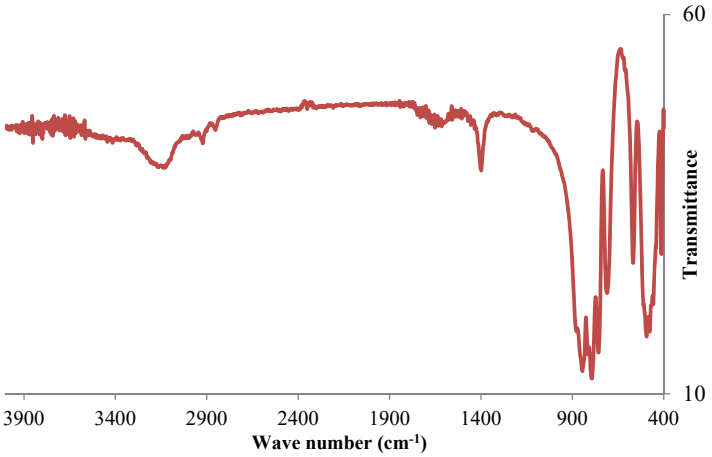

Fig. 5. FTIR spectrum of S_3.

Fig. 5 show the FTIR spectrum of S_3. There are some peaks at around 476, 518, 703, 754, 788, 803 and 1394 cm^{-1}. The strong bands at 476 and 518 cm^{-1} are assigned to the As–$O_{bridging}$ stretches. The band at about 754 cm^{-1} is attributed to the symmetric As–$O_{terminal}$ stretches. The band at around 803 cm^{-1} is assigned to doubly degenerate stretching vibrations of As-O bonds [10-13].

CONCLUSION

In this work, $As_2Ni_3O_8$ nanomaterial was synthesized via a facile solid state method. Two reaction parameter including raw material type and reaction temperature were investigated for the synthesis of the targets. PXRD patterns and structural analyses done by the *FullProf* program employing profile matching showed that nickel source in the reaction mixture had a main influence on the crystal size, growth and purity of the obtained targets. In the present work, we found that nickel nitrate created a highly crystalline and pure $As_2Ni_3O_8$ structures. However nickel acetate created the targets with lower purity and crystal phase growth, it produced that the samples with smaller crystallite sizes. Reaction temperature changing showed that the parameter affected the crystal growth amount of the obtained material. In this case, increasing the reaction temperature decreased the crystal growth of the target. It showed that the crystal phase of the sample was unstable at the higher temperature than 850 °C. Also, increasing the parameter couldn't improve the purity of the targets considerably when nickel acetate was used. FESEM images showed the obtained materials had sponge morphology. The data showed that increasing the reaction temperature could only decrease the particle size of the target and didn't change the morphology of the samples. Also, the direct optical band gaps were calculated and related to the reaction temperature. It was found that the band gaps were decreased with increasing the reaction temperature from 850 °C to 950 °C.

CONFLICT OF INTEREST

The authors declare that there is no conflict of interests regarding the publication of this manuscript.

REFERENCES

[1] M. El-Kemary, N. Nagy, I. El-Mehasse, Mater. Sci. Semicond. Process, 16, 1747 (2013).
[2] A. Rahdar, M. Aliahmad, Y, Azizi, J. Nanostructures. 5, 145 (2015).
[3] M. Riazian, Int. Nano Dimens. 5, 123 (2014).
[4] F. Zahraei, K. Rahimi, A. Yazdani, Int. J. Nano Dimens., 6, 371 (2015).
[5] S. Khanahmadzadeh, F. Barikan, Int. J. Nano Dimens., 5 365 (2014).
[6] S.C. Grund, K. Hanusch, H.U. Wolf, Arsenic and Arsenic Compounds, Ullmann's Encyclopedia of Industrial Chemistry", Weinheim: Wiley-VCH, doi:10.1002/14356007.a03_113.pub2 (2005).
[7] S. Gibaud, G. Jaouen Top. Organomet. Chem., 32, 1 (2010).
[8] J. Barbier, C. Frampton, Acta Crystallographica, Section B., 47, 457 (1991).
[9] J. Pascual, J. Camassel, Phys. Rev. B: Solid State. 18, 5606 (1978).
[10] A. Bishay, C. Maghrabi, Physics and Chemistry of Glasses. 10, 1 (1969).
[11] G. Srinivisa Rao, N. Veeraiah, Journal of Alloys Compounds. 327, 52 (2001)
[12] A.G. Nord, P. Kierkegaard, T. Stefanidis, J. Baran, Chem. Commun. 5, 1 (1988).
[13] T. Đorđevi´c, A. Wittwer, Z. Jagli˘ci´c, I. Djerdj, RSC Adv. 5, 18280 (2015).